Surface-enhanced Raman scattering of SnO_2 bulk material and colloidal solutions

Enza Fazio, Fortunato Neri, and Salvatore Savasta
Dipartimento di Fisica della Materia e Ingegneria Elettronica, Universita degli Studi di Messina, Viale F. Stagno d'Alcontres 31, 98166 Messina, Italy

Salvatore Spadaro
Advanced and Nano Materials Research s.r.l., Viale F. Stagno d'Alcontres 31, I-98166 Messina, Italy

Sebastiano Trusso*
CNR-IPCF Istituto per i Processi Chimico-Fisici, Viale F. Stagno d'Alcontres 37, 98158 Messina, Italy
(Received 12 December 2011; revised manuscript received 5 March 2012; published 14 May 2012)

Surface-enhanced Raman scattering (SERS) effects on tin dioxide in the form of bulk material, nanostructured thin films, and colloidal solutions were investigated. Raman spectra are characterized by the three Raman scattering peaks at 478, 633, and 776 cm^{-1}, assigned to the E_g, A_{1g}, and B_{2g} modes, typical of rutile SnO_2. In the presence of the silver nanoparticles, in addition to the enhancement intensity of some of the fundamental tin dioxide rutile Raman features, the appearance of a new Raman scattering peak at about 600 cm^{-1} is observed. These spectral features are observed, in the presence of silver nanoparticles, also in other SnO_2-based systems such as pulsed laser deposited thin films, with different stoichiometry, and in water colloidal solutions. The observed SERS effects are explained in terms of electric field gradient mechanism that are generated near a metal surface. In particular, the appearance of a peak near 600 cm^{-1} is attributed to the Raman activation of the infrared E_u transverse optical mode.

DOI: 10.1103/PhysRevB.85.195423 PACS number(s): 78.30.−j, 79.20.Eb, 78.67.Bf

I. INTRODUCTION

In the last decade, there has been an increasing interest in materials that can be used as surface-enhanced Raman scattering (SERS) substrate capable of appropriate levels of detection to allow the identification of trace constituents (for example, drug compounds recovered from surface contaminations). The enhancement of the Raman signal is mainly achieved by coupling the vibrational modes of the analyte molecule with the electromagnetic field generated at a metallic nanostructure, usually made of gold or silver, upon excitation with light of appropriate energy.[1–6] Moreover, recently, the use of a chemically inert shell coating around gold nanoparticles allows us to protect the SERS-active nanostructure, determining a much higher detection sensitivity and an increased field of application.[7] Nevertheless, along with the signal amplification, other spectral effects are often found, the nature of which is strictly connected to the material under SERS analysis.

In this paper, we investigate the modifications of the Raman spectral response of SnO_2 induced by silver nanoparticles. The high stability, the wide band gap, the high sensitivity, and the ability of SnO_2 to be integrated onto micromachined substrates make it a good candidate for the fabrication of dye-based solar cells, transistors, electrode materials, catalytic or electrochromic devices, and also miniaturized, ultrasensitive gas sensors due to its high reactivity with environmental gases.[8–12] Since the sensing properties of solid-state gas sensors are directly related to the surface area, the reduction of SnO_2 grain size leads to a much higher surface-to-bulk ratio, thus enhancing both the properties and performance of the devices. In an effort to overcome some of the SnO_2 technological performance limitations, a systematic study of its structural properties is crucial. As is well known, position, linewidth, and line shape of the Raman peaks are very sensitive to the local arrangements of structured and inhomogeneous materials.[13] Hence, Raman spectroscopy results to be an effective, simple, and nondestructive technique to characterize SnO_2 microstructures and nanostructures. Anomalous Raman spectra, where some IR allowed vibrations become Raman active, were observed in SnO_2 nanowires or SnO_2 nanostructures.[14–16] These findings were related to the grain size, film roughness, and, more generally, to structural disorder, but their origin was not exactly determined.

In addition to the spectral intensity enhancement, SERS determines the shifting and the broadening of the fundamental vibrational Raman modes as well as the appearance of new features. Generally, the SERS-induced occurrence of Raman forbidden peaks has been attributed to the lowering of the symmetry of the investigated molecules due to the formation of bonds at the metallic surface or to the presence of a steep field gradient close to the nanoparticle's metal surfaces.[17–19]

Here, we present Raman scattering spectra of SnO_2 bulk material and nanostructured thin films in the presence of silver nanoparticles. We find the appearance of new Raman-type lines either in SnO_2 bulk material and in nanostructured thin films, induced by silver nanoparticles. Experimental data from infrared absorption, x-ray diffraction (XRD), and Raman spectra, taken on different samples, provide precise indications about the electromagnetic origin of the observed effect. In particular, the electric gradient field Raman mechanism (GFR) occurring in the near-field region of the metallic nanoparticles can explain the experimental evidences. Moreover, we show that this effect is also present in colloidal solutions.

II. EXPERIMENTAL SECTION

A. Sample preparation and characterization

SERS experiments were carried out on different kinds of SnO_2 material: hot pressed pellet, pulsed laser deposited

thin films, and water colloidal solutions containing either micrometric- or nanometric-sized particles. Pellets were obtained by hot pressing commercial micrometric-sized powder purchased from Goodfellow. The pulsed laser deposited (PLD) SnO_2 thin films were prepared in a vacuum chamber using a 248-nm KrF laser beam focused at an incidence angle of 45° on the surface of a hot pressed SnO_2 pellets used as the target. The process was carried out at a substrate temperature of 470 K with a laser fluence of 1.0 J cm^{-2} in a controlled high-purity oxygen gas background atmosphere. The two samples studied here were grown at the oxygen pressure of 1.3 and 13.3 Pa. The film thickness was around 100 nm, while the oxygen content x, estimated by x-ray photoelectron spectroscopy, was 1.8 and 2.2, respectively. Further details on the experimental procedures and film properties were reported elsewhere.[20–22] SnO_2 water colloidal solutions were prepared following two different procedures: (1) by irradiating a high-purity metallic tin target, immersed in distilled water, with the second harmonic of a Nd:YAG laser (wavelength 532 nm, pulse width 5 ns, repetition rate 10 Hz) at the laser fluence of 1.0 J cm^{-2}, for typical irradiation times of 20 min; (2) dispersing 1.5 mg of SnO_2 micrometric-sized powder in 6 mL of pure water. Silver nanoparticle (NP) colloidal solutions were prepared in water ablating a high-purity silver target, at the laser fluence of 0.7 J cm^{-2} for a time of 20 min. To carry out transmission electron microscopy (TEM) and x-ray diffraction measurements, a few drops of the SnO_2 solutions were casted on carbon-coated copper grids and silicon substrates, respectively. TEM images were taken by a transmission electron microscope (model JEOL-JEM 2010) operating at an accelerating voltage of 200 kV, while XRD patterns were recorded, in the 2θ range from 20° to 80°, using a Bruker D8 advance x-ray diffractometer with the Cu K_α radiation (1.5406 ° Å). Fourier transform infrared transmission (FTIR) measurements of SnO_2 in KBr pellet were carried out using a Perkin-Elmer FTIR spectrophotometer. UV-vis optical transmission measurements of the silver NP solutions were carried out by a Perkin-Elmer LAMBDA 2 spectrophotometer in the 190–1000 nm range. The estimated Ag particle size was 20 nm, as determined from the position and the full width at half maximum (FWHM) of the surface plasmon resonance absorption peak and confirmed by the TEM imaging analysis.

B. SERS measurements

SERS measurements were performed on the surface of the hot pressed pellet and of the PLD deposited thin films after silver colloidal solutions were airbrush sprayed onto their surfaces. SERS measurements on the colloidal SnO_2 solutions were performed by adding 3 ml of the silver colloid to an equivalent volume of the SnO_2 solution one. A dilution study was carried out by progressively adding 3, 4, 5, and 6 ml of distilled water to the Ag-SnO_2 colloid. Raman scattering measurements were carried out in a backscattering geometry by means of a confocal micro-Raman apparatus focusing the 632.8-nm line of a He-Ne laser on the solid samples surface through the 50× objective of a microscope. Raman spectra from the colloidal solutions were collected using a 10× Mitutoyo infinity-corrected long working distance microscope objective. In both cases, backscattered radiation was collected by the same microscope optics, dispersed by a Jobin-Yvon Triax 320 monochromator equipped with a 1800 line/mm holographic grating and detected with a LN_2 cooled charged coupled device (CCD) sensor. All the shown spectra are normalized using their integration times.

III. RESULTS AND DISCUSSION

Tin dioxide in the rutile form belongs to the symmetry space group D_{4h}.[23–28] The 6 unit-cell atoms give rise to 18 vibrational modes. Two modes are infrared active (the single A_{2u} and the triply degenerate E_u), four are Raman active (the three nondegenerate A_{1g}, B_{1g}, B_{2g} modes and the doubly degenerate E_g one), and two others are silent (the A_{2g} and B_{1u} modes). The A_{1g} mode is a vibration along the c axis, while the E_u mode involves movements in the xy plane.[29–35] Figures 1(a) and 1(b) show the FTIR and the Raman spectra of the KBr/SnO_2 and the hot pressed SnO_2 pellets, respectively. Infrared transmission spectrum shows a broad band in the 400–800 cm^{-1} region, typical of a SnO_2 system.[36] In particular, it is characterized by a feature peaked around 600 cm^{-1} and attributed to the E_u transverse optical (TO) phonon mode,[37] and positions of the TO and longitudinal optical (LO) A_{2u} modes are also indicated.[38] The Raman spectrum is characterized by the presence of three peaks located at about 478, 633, and 776 cm^{-1} corresponding to the E_g, A_{1g}, and B_{2g} modes in good agreement with those observed in a single-crystal SnO_2 or polymicrocrystalline films.[39] Three broader and less intense bands can be observed at 350 $cm^{-1}$and between 400 and 800 cm^{-1}. They were identified as belonging to surface and acoustic modes, respectively.[37,40] In the same figure, the Raman spectrum collected on the hot pressed SnO_2 pellet

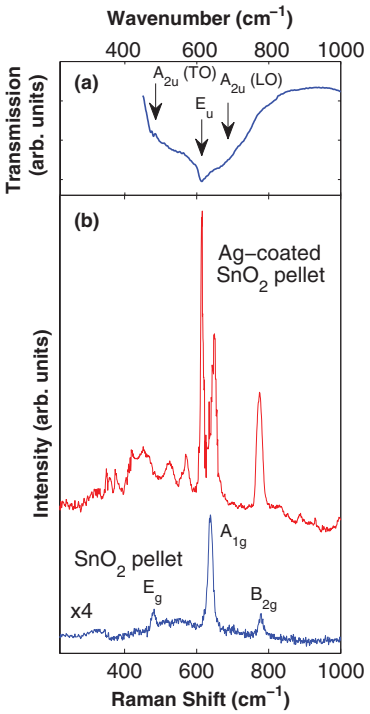

FIG. 1. (Color online) (a) FTIR spectrum of SnO_2 pellet; (b) Raman spectra of SnO_2 and Ag-coated SnO_2 pellet.

surface after the colloidal Ag airbrush spraying procedure is shown. Aside from the above reported three fundamental Raman modes, a new very intense peak at about 615 cm^{-1} is evident. Furthermore, other less intense peaks are present in the low wave-number portion of the spectrum at about 350, 374, 419, 482, and 524 cm^{-1}. The origin of the intense peak observed at 615 cm^{-1} could be attributed to the presence of the amorphous SnO_2 phase, even if, generally, a broad Raman band related to the amorphous phase is located at about 570 cm^{-1}.[41] Nevertheless, its position, narrow linewidth, and intensity, greater than the A_{1g} one, rule out such an attribution.

Another interesting effect of the presence of the silver NPs on the samples surface is the enhancement of the B_{2g} mode related peak, the intensity of which becomes comparable to that of A_{1g}. Otherwise, the E_g mode peak intensity resulted unaffected, being hindered by the appearance of the above-mentioned low-frequency peaks. Concerning the observed low wave-number peaks, their origin is still unclear and debated in literature. In the low-dimensional SnO_2 systems, their presence was associated to the activation of Raman modes as a consequence of disorder or size effects.[16,41] Taking into account that the hot pressed pellet was obtained from stoichiometric powders with particles having typical dimensions in the micrometric range, we can safely rule out any size effect. Moreover, it is worth mentioning that we are able to detect such bands only in presence of the silver NPs. The same silver NPs deposition procedure was performed on the surface of two SnO_x thin films grown by pulsed laser deposition at different deposition conditions. The films are characterized by different oxygen content x, i.e., 1.8 and 2.2 as determined by x-ray photoemission spectroscopy (XPS) measurements. The different oxygen content arose from the oxygen partial pressure (i.e., 1.3 and 13.3 Pa) at which the samples were grown. More details about the growth process can be found in Trusso *et al.*.[20] The corresponding Raman spectra are shown in Fig. 2. In the Raman spectra of the as-deposited samples, only the A_{1g} peak is easily distinguishable, its linewidth being narrower for the sample

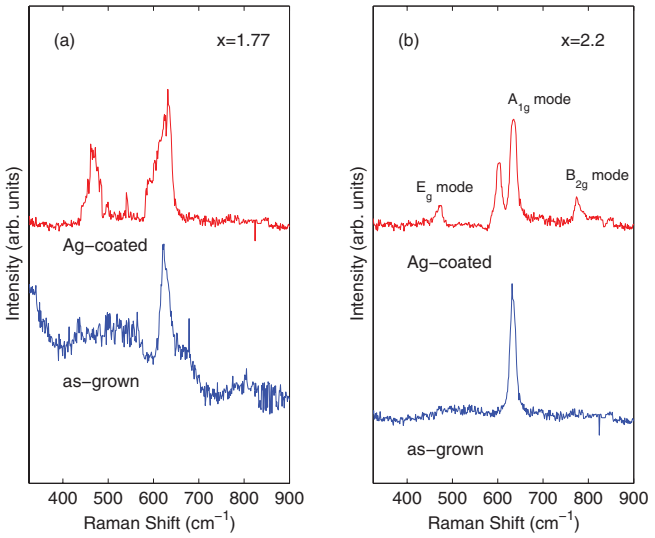

FIG. 2. (Color online) Raman spectra of SnO_x and Ag-coated SnO_x PLD grown samples.

with $x = 2.2$. A broad and structureless band is also barely visible in the 400–600 cm^{-1} region for both the samples. After the silver colloidal solution was sprayed on the film surface, the corresponding Raman spectra resulted very different. In the substoichiometric film, the E_g mode becomes visible, while the A_{1g} mode related band widens showing a shoulder on the low wave-number side [see Fig. 2(a)]. Concerning the other film, two effects are evident: the appearing of the E_g and B_{2g} mode related bands, together with a peak at about 600 cm^{-1}, as already observed in the Raman spectra of the hot pressed pellet. It should be noted that, at the surface of the substoichiometric film, the presence of oxygen vacancies can be envisaged. Taking into account that the E_g mode originated by the vibration of two oxygen atoms along the c axis, but in opposite direction, such a mode is more sensitive to oxygen vacancies than the other modes: the broad bump observed at around 500 cm^{-1} for the E_g mode proves this point.

As reported in a previous work,[22] all the PLD deposited films are composed of nanoparticles exceeding 10 nm in size and essentially with a tetragonal rutile crystalline structure. From the analysis of selected-area electron diffraction (SAED) patterns, it was shown that the tetragonal unit cell shrinks along both the principal axes when the compositional parameter x gets smaller, i.e., upon increasing the number of octahedrally arranged vacant sites of the oxygen atoms. Hence, we are reasonably confident that, for the substoichiometric film, the appearance of the new peak near the A_{1g} mode and the marked enhancement of the E_g one may be due in part to the surface defect states, which are easily linked with the A_g ones. On the other hand, for the $x = 2.2$ stoichiometry sample, the well-defined and shrinked features around 600 cm^{-1} and the TEM imaging analysis[22] suggest that the observation of such vibrational mode is not due to the presence of structural defects. The investigation was extended to systems consisting of SnO_2 colloidal solutions prepared by different methods. A first colloidal solution was prepared simply by dispersing SnO_2 micrometric powder in distilled water, while a second colloidal solution was prepared by pulsed laser ablating a pure tin target in water, following the same procedure adopted in the case of the Ag nanoparticles. The SnO_2 particle formation is due to reactions between oxygen atoms, originating from dissociation of water molecules in the laser-generated plasma region, and tin ones coming ejected from the target by the focused laser pulse. In this latter case, the size of the SnO_2 colloidal particle resulted in the nanometer range.

In Fig. 3, the Raman scattering features for water dispersed micrometric SnO_2 powder are shown. In the same figure, the Raman spectrum acquired after the addition of the silver NPs colloidal solution is reported. The pure micrometric SnO_2 powder solution spectrum is almost identical to that acquired on the surface of the pellet (see Fig. 1). Looking at the Raman spectrum of the silver colloid SnO_2 powder mixed solution, the appearance of two peaks at about 300 and 600 cm^{-1} can be envisaged. Furthermore, the peak centered at about 478 cm^{-1} appears more structured with respect to that observed in the absence of silver nanoparticles. A structural characterization of the different SnO_2 systems was performed by TEM imaging and SAED measurements. The results are reported in Fig. 4, where TEM images and SAED patterns of dried SnO_2 nanoparticles are shown. In the TEM, image clusters, 25 nm

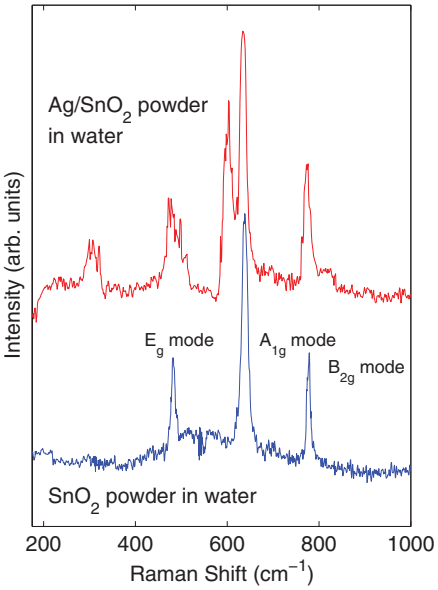

FIG. 3. (Color online) Raman spectra of SnO_2 and Ag-SnO_2 colloidal water solutions.

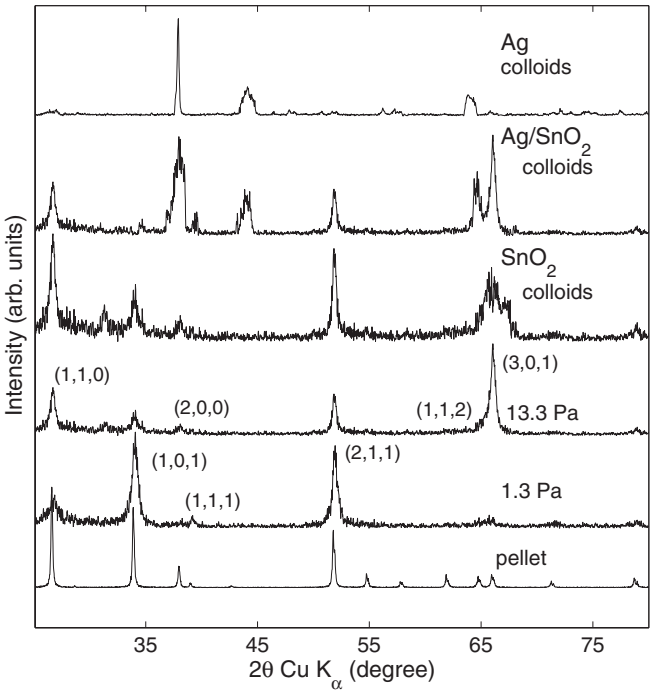

FIG. 5. XRD spectra of all the investigated samples.

in size, composed by nearly spherical nanoparticles can be observed. As shown by the high-resolution TEM (HRTEM) image, 6–10 nm sized nanoparticles are present; in some cases, they overlap and are connected with two or three neighbors through necks. SAED pattern measurements were carried out to look at the crystallographic structure of the colloids. SAED patterns show the (1,1,0), (1,0,1), and (2,1,1) rings typical of the tetragonal rutile SnO_2 structure. The widespread halo can not be associated with reasonable certainty to the SnO_2 amorphous phase since the carbon membranes, onto which the colloidal solution was deposited, could contribute to the total homogeneous and isotropic diffraction.

Looking for a confirmation concerning the crystallographic structure of the samples, XRD measurements were carried out. In Fig. 5, the XRD spectrum of the SnO_2 colloids and of the samples deposited in oxygen atmosphere are shown for comparison. The normal tetragonal rutile structure with major reflections along the (2,1,1), (1,0,1), and (3,0,1) planes occurs for all the samples. For the SnO_2 colloids, the reflections (2,1,1) and (1,1,0) become predominant. The same analysis, carried out for the Ag-SnO_2 mixed colloids, shows, in addition, the typical silver phase features corresponding to the (1,1,1), (0,0,2), and (2,2,0) reflections referred to the peaks occurring around 37.95°, 44.15°, and 64.30° Å. Then, we have no evidence that the chemistry of the tin oxide material is affected by the presence of the silver nanoparticles.

The Raman spectrum of the nanostructured SnO_2 colloidal solution is shown in Fig. 6(a). The main features are the well-defined peak centered around 630 cm^{-1}, while the contributions related to the E_g and B_{2g} are barely visible. By adding a silver nanoparticle solution, in addition to the enhancement intensity of some of the fundamental tin dioxide rutile Raman features, a new well-defined peak toward 600 cm^{-1} appears and grows in intensity at the expense of the A_{1g} mode contribution.

In order to rule out any chemical effect between Ag atoms and the surface of SnO_2 particles, we diluted the

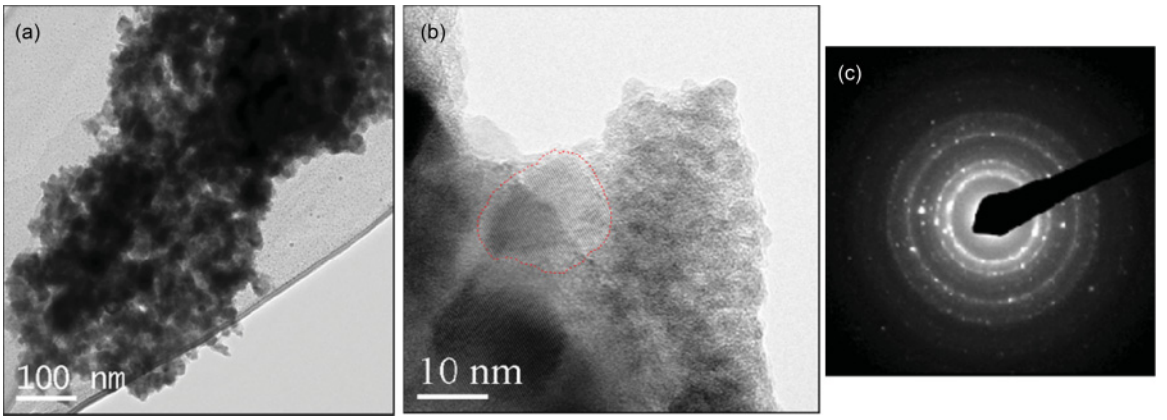

FIG. 4. (Color online) TEM images and SAED patterns of the SnO_2 colloidal solutions.

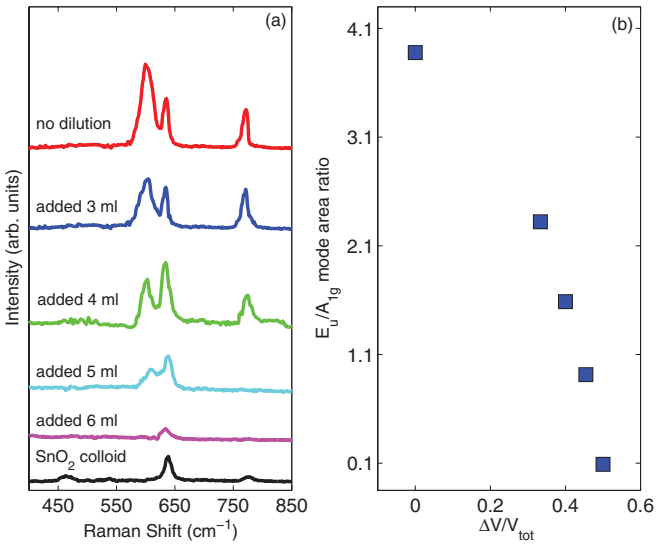

FIG. 6. (Color online) (a) Raman spectra of Ag-SnO_2 colloidal solutions; (b) E_u/A_{1g} TO vibrational mode area ratio vs $\Delta V/V_{\text{tot}}$ where ΔV is the water volume added to the original colloidal solution and V_{tot} the resulting total volume.

Ag-SnO_2 solution by adding progressively few ml of water. The resulting spectra are reported in Fig. 6(a) together with the spectrum of the SnO_2 colloid. If the activation of the peak observed around 600 cm^{-1} should have a chemical origin (with the formation, for example, of Ag-SnO_2 complexes), it should still be present after dilution. On the other side, if the effect has an electromagnetic origin, i.e., due to the strong electric field enhancement and/or to its gradient around the metallic nanoparticles induced by localized surface plasmon resonances, the behavior should be different. In this latter case, the activation of the normally forbidden Raman mode is effective only when the SnO_2 nanoparticles are, at most, only a few nanometers separated by the silver ones. Hence, in a colloidal solution, the effect should be proportional to the number of effective collisions between the metallic and the SnO_2 nanoparticles, during the spectra acquisition time, collisions which are inversely proportional to the added water volume. Indeed, Fig. 6(a) shows that, upon increasing dilution, the peak intensity of the normally forbidden Raman mode decreases. Particularly, by increasing dilution, the spectra in Fig. 6(a) tend toward the ones in the absence of metallic nanoparticles, displaying a fully reversible behavior, so ruling out the presence of chemical processes activating the Raman peak. In addition, Fig. 6(b) shows that the ratio between the areas of the E_u and A_{1g} modes decreases with the quantity $\Delta V/V_{\text{tot}}$, where ΔV is the water volume added to the original colloidal solution and V_{tot} is the resulting total volume. Thus, the reversibility of the process versus the H_2O dilution [Fig. 6(b)] indicates that no formation of Ag-SnO_2 complexes occurs, in good agreement with the XRD data. The absence of significant SERS-induced frequency shifts in the Raman spectra, the reversibility of the effect upon dilution and the XRD results, suggests a negligible chemical interaction between the compound and the silver nanoparticles. Overall, this spectral effect is independent on the SnO_2 size (bulk or nanostructure) or on the surrounding matrix (i.e., solid or water solution) in which the oxide is found. The observation of these anomalous Raman spectra depends only on the presence of the Ag nanoparticles. Thus, the appearance of the normally Raman forbidden mode around 600 cm^{-1} can, more likely, be attributed to the electromagnetic effects induced by the silver nanoparticles. In the last years it has been shown that the appearance of normally forbidden vibration modes can be explained by the presence of an electric field gradient in the near-field region of metallic nanoparticles. In general, the SERS-induced occurrence of Raman forbidden peaks has been attributed to the lowering of the symmetry of the investigated molecules due to the formation of bonds at the metallic surface or to the presence of a steep field gradient close to the nanoparticles metal surfaces.[42,43]

When the electric field varies over the length of the SnO_2 bond, the Raman signal can depend upon the polarizability times the field gradient in addition to the usual dependence on the polarizability gradient. The strong field gradient generated at the metallic surface, as already observed in the SERS spectrum of benzene,[42,43] shifts the potential energy of the induced dipole in an asymmetric manner, leading to a coupling with the applied field that lacks a center of symmetry. Overall, the loss of a center of symmetry eliminates the requirements of the mutual exclusion rule, which dictates that modes can only be either Raman or infrared active. Thus, modes that would normally appear only in the infrared spectrum can appear in the SERS spectrum.[44–46] A similar mechanism can occur when the SnO_2 colloidal nanoparticles are at most only a few nanometers separated by the silver ones. The strong electric field gradient near the silver nanoparticles permits a different coupling mechanism between the optical electric field and the vibration. The selection rules for this process differ markedly from the usual Raman selection rules, and the prefactors favor Raman-type observation of strong infrared (not normally Raman active) vibrations. Transitions in vibration levels due to coupling with a radiation field are described by the perturbation Hamiltonian $H = \mu E$, where μ is the dipole moment and E is the electric field. The first-order expansion of the dipole moment μ in the coordinate of vibration Q is given by the following expression:[47,48]

$$\mu_a = \left[\left(\frac{d\mu_\alpha^p}{dQ}\right) + \left(\frac{d\alpha_{ab}}{dQ}\right)E_b + \alpha_{ab}\left(\frac{dE_b}{dQ}\right)\right]Q + \cdots, \tag{1}$$

where the three terms yield the infrared absorption, the Raman, and the gradient field Raman (GFR) contributions, respectively. Compared to the classical treatment, the new GFR term takes into account that the electric field E can not be removed from the derivative term since E, varying very rapidly near the metal surface, depends on the coordinate Q. In particular, the ratio of the GFR to the Raman terms is approximated as α/a, a being a molecular dimension. The jellium approximation of Feibelman[49] indicates that the electric field in proximity of a metallic surface varies by nearly its full amplitude over 0.2 nm. The GFR/Raman terms ratio is expected to be $\approx$1. Figure 7 provides a schematic view of the GFR effect. In order that the molecular vibration be able to inelastic scatter radiation, there must be a change in

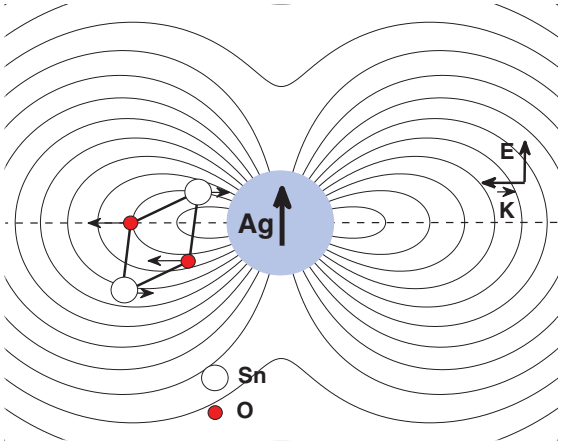

FIG. 7. (Color online) Schematic view of the gradient field Raman (GFR) effect.

the dipole moment during the vibration [see Eq. (1)]. Figure 7 shows a Raman forbidden stretch of the SnO_2 molecule. In this asymmetric stretch, the electrons are more easily polarized in the bonds that expand but are less easily polarized in the bond that compresses (as indicated by the arrows). As a consequence, there is no overall change in the polarizability and the mode is Raman inactive. Otherwise, the strong electric field gradient induced by the metallic nanoparticles determines an overall change of the dipole moment during the vibration, even in the absence of a polarizability change as quantitatively described by the third term in Eq. (1). In the specific case of a subwavelength metallic sphere as displayed in Fig. 7, the electric field changes very rapidly as $1/R^3$, R being the distance from its center. This theoretical analysis confirms that the observed appearance of the Raman forbidden peak occurs only when SnO_2 and silver particles are in close proximity. In the case of Ag-SnO_2 colloidal solutions, this effect originates from effective collisions between the metallic and the SnO_2 nanoparticles, as a consequence of Brownian motion during the spectra acquisition time. An additional GFR-like contribution may arise from the quadrupole Raman term.[48] Since in Eq. (1) the polarizability multiplies the electric-field gradient term, the GFR effect will be proportional to the polarizability and, therefore, it is even more evident in molecules with larger polarizability, such as those characterized by ionic bonds. Among these materials, SnO_2 has a fairly high degree of ionic bonds.[50] This intrinsic characteristic of the material is another element that leads us to believe that it is reasonable to adopt the electric field gradient mechanism to explain the observed SERS effects.

IV. CONCLUSIONS

Significant surface-enhanced Raman scattering (SERS) effects from SnO_2 in the form of bulk material, nanostructured thin films, and colloidal solutions have been reported. In the presence of silver nanoparticles, aside from the intensity enhancement of some of the fundamental SnO_2 rutile Raman features, the appearance of a new Raman-type line at about 600 cm^{-1} is observed. It was found that the appearance of the new Raman peak depends only on the presence of the Ag nanoparticles, independently on the SnO_2 grain size, and on the surrounding matrix in which the oxide is found. Such a Raman feature was attributed to the infrared active E_u TO vibration mode, normally Raman inactive. Experimental data from infrared absorption, XRD, and Raman spectra, taken on different samples, provide precise indications about the electromagnetic origin of the observed effect. In particular, the reported SERS measurements can be explained in terms of the gradient field Raman mechanism. Most remarkably, we demonstrated the effectiveness of such GFR effect in colloidal solutions. Furthermore, the investigations will deserve an extension to other systems in order to check if the GFR mechanism can be used to explain the SERS-induced spectral modifications.

*trusso@me.cnr.it

[1] I. A. Larmour, K. Faulds, and D. Graham, J. Phys. Chem. C **114**, 13249 (2010).
[2] M. A. Khan, T. P. Hogan, and B. Shanker, J. Raman Spectrosc. **39**, 893 (2008).
[3] M. Moskovits, J. Raman Spectrosc. **36**, 485 (2005).
[4] E. Le Ru and P. Etchegoin, *Principles of Surface Enhanced Raman Spectroscopy* (Elsevier, Amsterdam, 2009).
[5] L. G. Quagliano, J. Am. Chem. Soc. **126**, 7393 (2004).
[6] W. Ye, D. Wang, H. Zhang, F. Zhou, and W. Liu, Electrochim. Acta **55**, 2004 (2010).
[7] J. F. Li, Y. F. Huang, Y. Ding, Z. L. Yang, S. B. Li, X. S. Zhou, F. R. Fan, W. Zhang, Z. Y. Zhou, D. Y. Wu, B. Ren, Z. L. Wang, and Z. Q. Tian, Nature (London) **464**, 392 (2010).
[8] A. Thurber, K. M. Reddy, and A. Punnoose, J. Appl. Phys. **105**, 07E706 (2009).
[9] B. Bahrami, A. Khodadadi, M. Kazemeini, and Y. Mortazavi, Sens. Actuators, B **133**, 352 (2008).
[10] R. Demir-Cakan, Y. S. Hu, M. Antonietti, J. Maier, and M. M. Titirici, Chem. Mater. **20**, 1227 (2008).
[11] Y. D. Wang, I. Djerdj, B. Smarsly, and M. Antonietti, Chem. Mater. **21**, 3202 (2009).
[12] H. X. Zhang, C. Feng, Y. C. Zhai, K. L. Jiang, Q. Q. Li, and S. S. Fan, Adv. Mater. **21**, 2299 (2009).
[13] D. A. Long, *The Raman Effect* (Wiley, Chichester, England, 2002).
[14] A. Diéguez, A. Romano-Rodríguez, A. Vilà, and J. R. Morante, J. Appl. Phys. **90**, 1550 (2001).
[15] J. Zuo, C. Xu, X. Liu, and C. Wang, J. Appl. Phys. **75**, 1835 (1994).
[16] Y. K. Liu, Y. Dong, and G. H. Guang, Chin. Phys. Lett. **21**, 156 (2004).
[17] A. R. Alvarez-Puebla and L. M. Liz-Marzan, Small **6**, 604 (2010).
[18] T. Kang, S. Hong, Y. Choi, and L. P. Lee, Small **6**, 2649 (2010).
[19] M. Sackmann and A. Materny, J. Raman Spectrosc. **37**, 305 (2006).
[20] S. Trusso, B. Fazio, E. Fazio, F. Barreca, and F. Neri, Thin Solid Films **518**, 5409 (2010).
[21] E. Fazio, F. Neri, R. Ruggeri, and S. Trusso, Radiat. Eff. Defects Solids **165**, 700 (2010).
[22] E. Fazio, F. Neri, R. Ruggeri, G. Sabatino, S. Trusso, and G. Mannino, Appl. Surf. Sci. **257**, 2520 (2010).

[23]S. P. S. Porto, P. A. Fleury, and T. C. Damen, Phys. Rev. **154**, 522 (1967).
[24]F. Gu, S. F. Wang, H. M. Cao, and C. Z. Li, Nanotechnology **19**, 095708 (2008).
[25]J. Zuo, C. Xu, X. Liu, and C. Wang, J. Appl. Phys. **75**, 1835 (1994).
[26]C. Wang, B. Lu, J. Zuo, S. Zhang, S. Tan, M. Suzuki, and W. T. Chase, Nanostruct. Mater. **5**, 489 (1995).
[27]J. Q. Hu, X. L. Ma, N. G. Shang, Z. Y. Xie, N. B. Wong, C. S. Lee, and S. T. Lee, J. Phys. Chem. B **106**, 3823 (2002).
[28]S. H. Sun, G. W. Meng, Y. W. Wang, T. Gao, M. G. Zhang, Y. T. Tian, X. S. Peng, and L. D. Zhang, Appl. Phys. A **76**, 287 (2003).
[29]M. E. Striefler and G. R. Borschi, Phys. Status Solidi B **67**, 143 (1975).
[30]R. S. Katiyar, P. Dawson, M. M. Hargreave, and G. R. Wilkinson, J. Phys. C: Solid State Phys. **4**, 2421 (1971).
[31]J. X. Zhou, M. S. Zhang, J. M. Hong, and Z. Yin, Solid State Commun. **138**, 242 (2006).
[32]P. S. Peercy and B. Morosin, Phys. Rev. B **7**, 2779 (1973).
[33]T. Sato and T. Asari, J. Phys. Soc. Jpn. **64**, 1193 (1995).
[34]L. Ying-Kai, D. Yi, and W. Guang-Hou, Chin Phys. Lett. **21**, 156 (2004).
[35]D. Shuo, L. J. Quan, and L. Y. Long, Chin Phys. **13**, 1854 (2004).
[36]L. Fraigi, D. G. Lamas, and N. E. W. de Reca, Nanostruct. Mater. **11**, 311 (1999).
[37]M. Batzill and U. Diebold, Prog. Surf. Sci. **79**, 47 (2005).
[38]B. Cheng, C. Xie, L. Fang, Y. Xiao, and S. Lei, Mater. Chem. Phys **129**, 713 (2011).
[39]Q. H. Wu, J. Song, and J. Li, Surf. Interface Anal. **40**, 1488 (2008).
[40]Rumyantseva *et al*., Chem. Mater. **17**, 893 (2005).
[41]F. H. Aragon, J. A. H. Coaquira, P. Hidalgo, S. W. da Silva, S. M. L. Brito, D. Gouvêa, and P. C. Morais, J. Raman Spectrosc. **42**, 1081 (2011).
[42]P. A. Lund, D. E. Tevault, and R. R. Smardzewski, J. Phys. Chem. **88**, 1731 (1984).
[43]A. Campion, V. M. Grizzle, D. R. Mullins, and J. K. Brown, J. Phys. Colloq. **44**, C10-341 (1983).
[44]A. Pinczuk and E. Burstein, Solid State Commun. **6**, 407 (1968).
[45]F. Schaffler and G. Abstreiter, Phys. Rev. B **34**, 4017 (1986).
[46]E. Smith and G. Dent, *Modern Raman Spectroscopy: A Practical Approach* (Wiley, New York, 2005).
[47]M. Moskovits, Rev. Mod. Phys. **57**, 783 (1985).
[48]E. J. Ayars, H. D. Hallen, and C. L. Jahncke, Phys. Rev. Lett. **85**, 4180 (2000).
[49]P. J. Feibelman, Phys. Rev. B **12**, 1319 (1975).
[50]J. Mimaki, T. Tsuchiya, and T. Yamanaka, Z. Kristallogr. **215**, 419 (2000).